Using the HYM code for numerical simulations of NSTX and FRC

Elena Belova

PPPL

June 20, 2014

HYM – HYbrid and MHD code

Applications

- NSTX
  - Sub-cyclotron frequency Alfven eigenmodes (GAE and CAE)
- ICC Theory and Modeling
  - 3D simulations of the MRX-magnetic arc experiments.
  - Hybrid simulations of spheromak merging
- FRC – Tri-Alpha collaboration
  - Effects of beam ions on stability
  - Rotation control
  - n=2 rotational and n=1 wobble modes

Code description

- 3-D nonlinear.
- Physical models:
  - Resistive MHD & Hall-MHD
  - Hybrid (fluid electrons, particle ions)
  - MHD/particle (one-fluid thermal plasma, + energetic particle ions)
  - Drift-kinetic particle electrons
- Full-orbit kinetic ions.
- For particles: delta-f / full-f numerical scheme.
- Parallel (3D domain decomposition, MPI)

PPPL
PRINCETON PLASMA PHYSICS LABORATORY

Self-consistent MHD + fast ions coupling scheme

Background plasma - fluid:

$$\rho \frac{d\mathbf{V}}{dt} = -\nabla p + (\mathbf{j} - \mathbf{j}_i) \times \mathbf{B} - n_i (\mathbf{E} - \eta \mathbf{j})$$

$$\mathbf{E} = -\mathbf{V} \times \mathbf{B} + \eta \mathbf{j}$$

$$\mathbf{B} = \mathbf{B}_0 + \nabla \times \mathbf{A}$$

$$\partial \mathbf{A} / \partial t = -\mathbf{E}$$

$$\mathbf{j} = \nabla \times \mathbf{B}$$

$$\partial p^{1/\gamma} / \partial t = -\nabla \cdot (\mathbf{V} p^{1/\gamma})$$

$$\partial \rho / \partial t = -\nabla \cdot (\mathbf{V} \rho)$$

Fast ions – delta-F scheme:

$$\frac{d\mathbf{x}}{dt} = \mathbf{v}$$

$$\frac{d\mathbf{v}}{dt} = \mathbf{E} - \eta \mathbf{j} + \mathbf{v} \times \mathbf{B}$$

$w = \delta F / F$ - particle weight

$$\frac{dw}{dt} = -(1 - w) \frac{d(\ln F_0)}{dt}$$

$$F_0 = F_0(\varepsilon, \mu, p_\phi)$$

ρ, $\mathbf{V}$ and p are bulk plasma density, velocity and pressure, n_i and $\mathbf{j}_i$ are fast ion density and current, $n_i << n$ – is assumed.

Correlation between strong GAE/CAE activity and enhanced electron transport has been observed in NSTX [Stutman, PRL 2009]

- Plasmas with rapid central electron transport show intense GAE activity (0.5-1.1MHz), while low-transport plasmas are GAE free.
- Flattening of the electron temperature profile with increased beam power.
- Correlation is also observed in experiments with the beam energy scanned between 60keV and 90 keV [Stutman, PRL 2009].
- Test particle simulations using the ORBIT code predict thermal electron transport due to orbit stochasticity in the presence of multiple core localized GAE modes [Gorelenkov, NF 2010].
- Anomalous electron transport potentially can have significant implications for future fusion devices, especially low aspect ratio tokamaks.

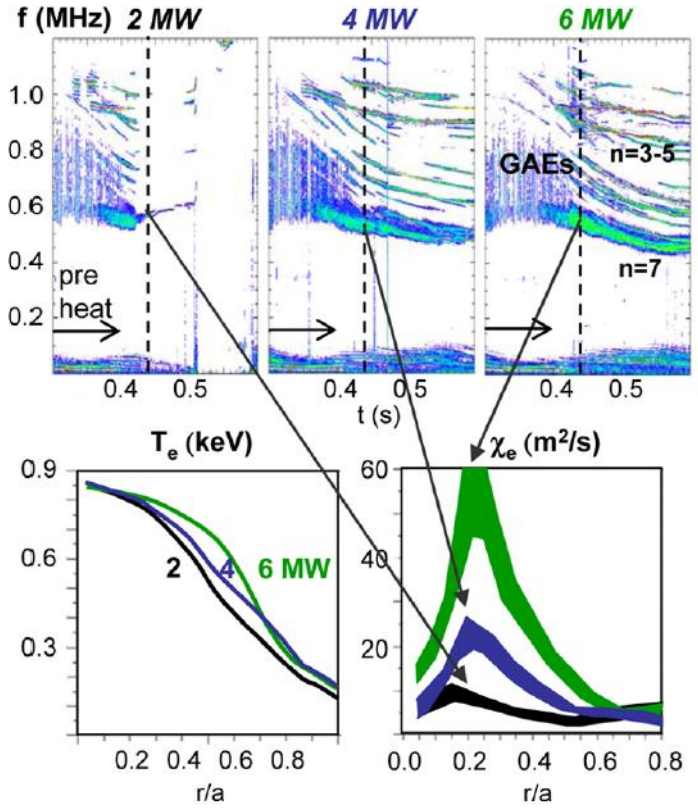

Correlation between GAE activity, T_e flattening, and central electron heat diffusivity χ_e in NSTX H modes with 2, 4, and 6MW neutral beam.

NSTX

PPPL PRINCETON PLASMA PHYSICS LABORATORY

GAE and CAE modes observed in NSTX shot # 141398

Experimental measurements

[N. Crocker, IAEA 2012, EX/P6-02]

- Detailed measurements of GAE and CAE modes amplitudes and mode structure were obtained for H-mode plasma in NSTX shot 141398.
- The modes have been identified as CAE modes for frequencies f>600 kHz, and small toroidal mode numbers |n|≤5.
- The modes have been identified as GAEs for f<600 kHz, and |n|~6-8 based on dispersion relations.

HYM simulations

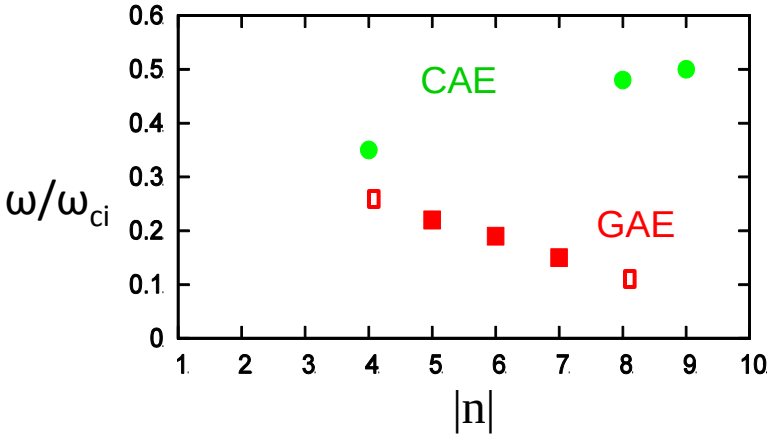

Frequency versus toroidal mode number for most unstable GAE (red) and CAE (green) modes, from HYM simulations for NSTX shot #141398. Frequency is normalized to ion cyclotron frequency at the axis f_{ci}=2.5MHz.

HYM simulations show that most unstable modes for n=5-7 are counter-rotating GAE modes, with shear Alfven wave polarization in the core and f= 380-550 kHz. The n=4 and n=8 and 9 modes are co-rotating CAE modes with f= 870-1200 kHz, which have been identified based on large compressional component of perturbed magnetic field.

Equilibrium calculations

Equilibrium distribution function $F_0 = F_1(v)F_2(\lambda)F_3(p_\phi)$

$$
\begin{aligned}
F_1(v) &= \frac{1}{v^3 + v_*^3}, \quad \text{for } v < v_0 \\
F_2(\lambda) &= \exp(-(\lambda - \lambda_0)^2/\Delta\lambda^2) \\
F_3(p_\phi) &= \frac{(p_\phi - p_0)^\beta}{(R_0 v - \psi_0 - p_0)^\beta}, \quad \text{for } p_\phi > p_0
\end{aligned}
$$

where $v_0 \approx 3v_A$, $v_* = v_0/\sqrt{3}$, $\lambda = \mu B_0/\varepsilon$ - pitch angle,
$\lambda_0 = 0.8 - 1$,
and $\mu = \mu_0 + \mu_1$ includes first-order corrections [Littlejohn'81]:

$$
\mu = \frac{(\mathbf{v}_\perp - \mathbf{v}_d)^2}{2B} - \frac{\mu_0 v_\parallel}{2B}[\hat{\mathbf{b}} \cdot \nabla \times \hat{\mathbf{b}} - 2(\hat{\mathbf{a}} \cdot \nabla \hat{\mathbf{b}}) \cdot \hat{\mathbf{c}}]
$$

$\mathbf{v}_d$ is magnetic gradient and curvature drift velocity, $\hat{\mathbf{c}} = \mathbf{v}_\perp/v_\perp$,
$\hat{\mathbf{a}} = \hat{\mathbf{b}} \times \hat{\mathbf{c}}$

n=8 CAE mode: effective potential well

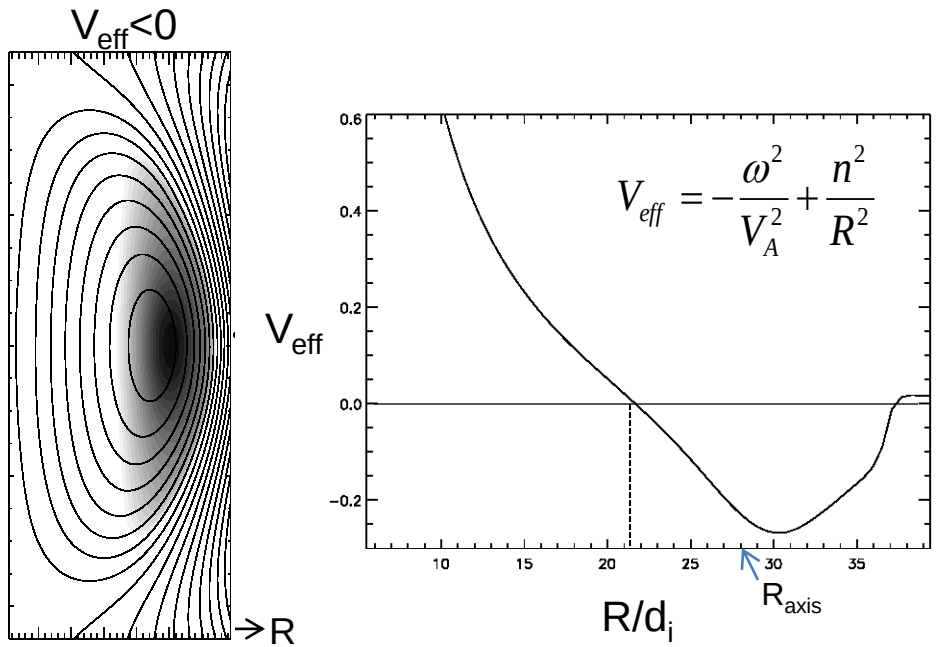

Contour plot and radial profile of the effective potential V_{eff} for n=8 CAE mode with $\omega=0.48\omega_{ci0}$. Mode can exist for $V_{eff} < 0$ with radial extent: 22<R<37 (major radius is normalized to ion skin depth d_i=3.93cm).

Approximate equation for CAE mode, assuming circular cross-section, and neglecting beam effects and coupling to SAW:

$$\frac{\partial^2 \delta B_\parallel}{\partial r^2} = V_{eff}\ \delta B_\parallel$$

$$V_{eff} = -\frac{\omega^2}{V_A^2} + k_\parallel^2$$

HYM simulations show unstable n=8 mode with $\omega=0.48\omega_{ci0}$ and $\gamma=0.004\omega_{ci0}$.

Effective potential well for n=8 mode is narrower and deeper than V_{eff} for n=4 resulting in more localized CAE mode with larger frequency.

Edge of CAE well coincides with resonance location → CAE/KAW coupling.

n=8 co-rotating CAE: mode structure

$\delta B_{||}$

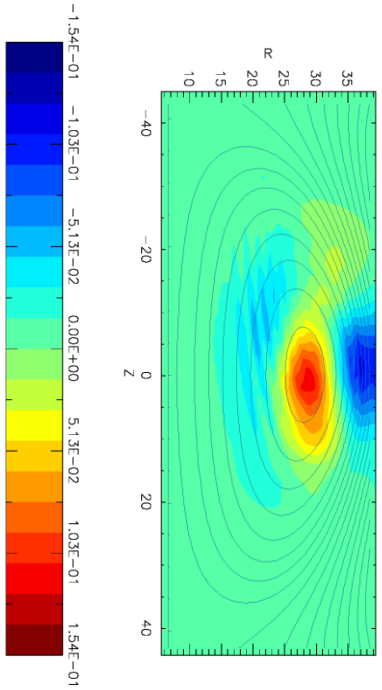

$|\delta B_{\perp}|$

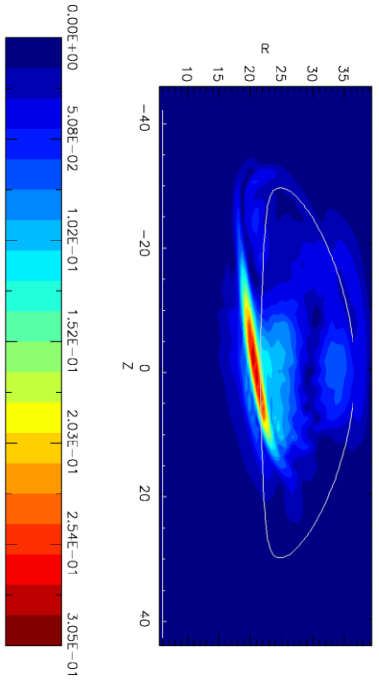

Higher-n co-rotating CAEs show resonant coupling to KAW. CAE mode peaks near magnetic axis, where $\delta B_{||} >> \delta B_{\perp}$, KAW is located at the resonance (solid contour line of $\omega_A (Z,R)=\omega_{CAE}$) on HFS.

Low-n and high-n CAE modes show coupling to KAW

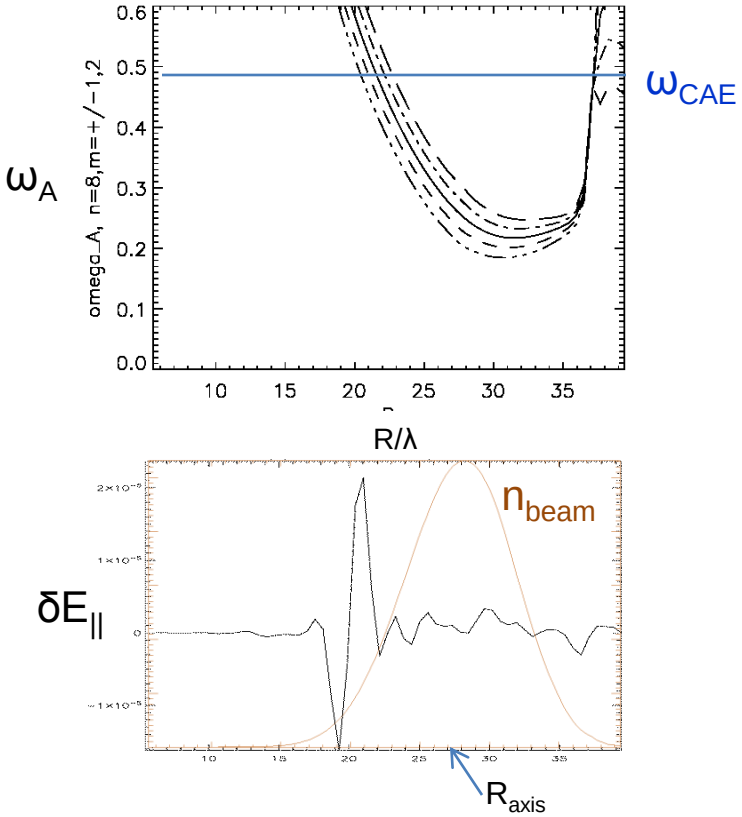

Radial profiles of Alfven continuum and $\delta E_{||}$ for n=8. Radial width of KAW is comparable to beam ions Larmor radius.

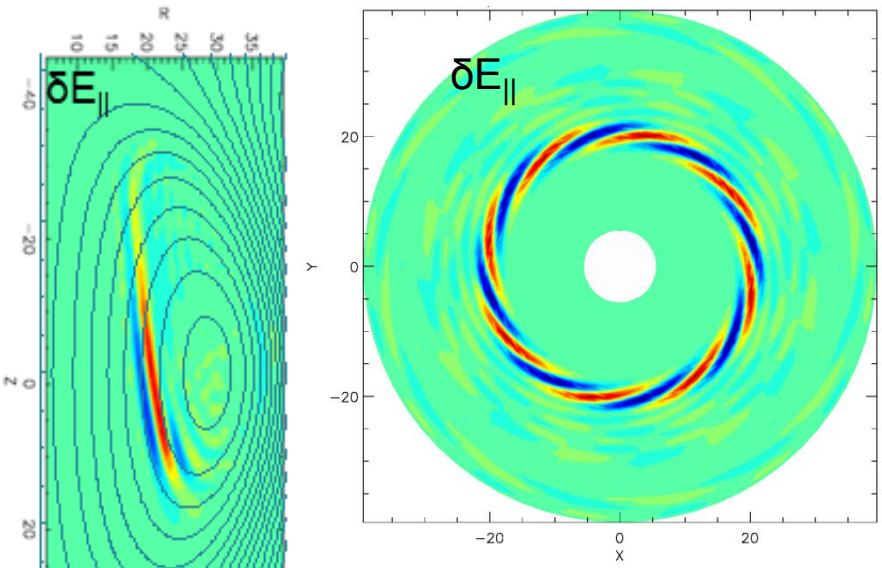

Poloidal and equatorial plane contour plots of $\delta E_{||}$, solid line is contour of $\omega_A(Z,R) = \omega_{CAE}$, where $\omega_A(Z,R) = V_A\, n/R$.

KAW can have strong effect on electron transport due to finite $\delta E_{||}$.

KAW dispersion relation

- assuming three-component plasma, Maxwellian ions with V_0=0, and including only adiabatic beam ions response (non-perturbative).

KAW in full kinetic model: $$\omega^2 = k_\parallel^2 V_A^2 \left(1 + \lambda_e + \frac{3}{4}\frac{n_i}{n_e}\lambda_i + \frac{3}{4}\frac{n_b}{n_e}\lambda_b - \frac{\omega^2}{\omega_{ci}^2} \right),$$

$$\text{where} \quad \lambda_\alpha = \frac{k_\perp^2 T_\alpha}{m_i \omega_{ci}^2}$$

KAW in HYM model: $$\omega^2 = k_\parallel^2 V_A^2 \left(1 + \frac{3}{4}\frac{n_b}{n_e}\lambda_b - \frac{n_b}{n_e}\frac{\omega^2}{\omega_{ci}^2} \right), \quad \lambda_b = \frac{k_\perp^2 T_b}{m_i \omega_{ci}^2}$$

- consistent with full kinetic in the limit $\lambda_e \to 0$, $\lambda_i \to 0$, and $\omega << \omega_{ci}$.

Scale-length for beam-KAW is the beam ion Larmor radius.

Relation between CAE/KAW and T_e flattening?

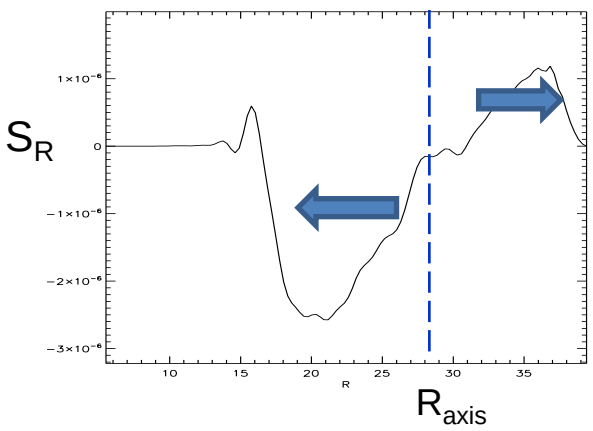

Radial component of quasilinear Poynting vector **S**=<**E**x**B**>. Energy flux is directed away from magnetic axis, ie from CAE to KAW.

Fraction of NBI power transferred to CAE can be estimated as:

$$P = 2\gamma \int (\delta B)^2/4\pi \, d^3x,$$

where $\delta B/B_0 = (0.9\text{-}3.4)\times 10^{-3}$ corresponds to measured displacement $|\xi| = 0.1\text{-}0.4$ mm [N.Crocker'13] (based on HYM-calculated linear mode structure for the n=4 CAE).

For γ/ω_{ci}=0.005-0.01, P= (0.013-0.4)MW,

- significant fraction of NBI energy can be transferred to several unstable CAEs of relatively large amplitudes.

Energy flux from the CAE to the KAW and dissipation at the resonance location can have a strong effect on the temperature profile.

Summary (NSTX)

- Unstable CAE modes couple with KAW on the HFS. Resonance with KAW is located at the edge of CAE well, and just inside beam ion density profile. Radial width of KAW is comparable to beam ion Larmor radius.
- A significant fraction of NBI energy can be transferred to several unstable CAEs: P~0.4MW for $\delta B/B_0 \sim 10^{-3}$.
- Energy flux from the CAE to KAW and dissipation at the resonant location can have direct effect on electron temperature profile.
- In addition, radially overlapping KAWs can strongly enhance plasma heat transport due to finite $\delta E_{||}$ and large width of resonant mode.
- Detailed comparison of the relative importance of the energy channelling and anomalous electron transport mechanisms will require fully nonlinear simulations, and will be performed in the future.

2D hybrid simulations of spheromak merging

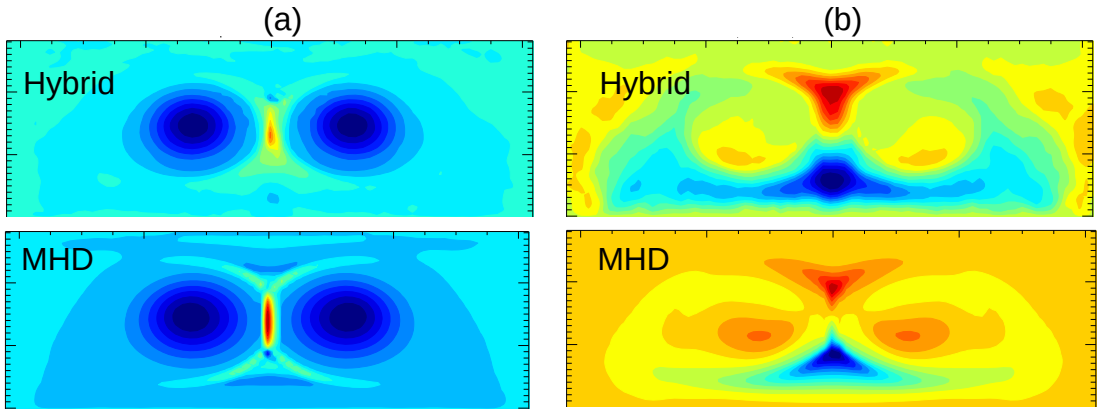

Contour plots of (a) toroidal current and (b) toroidal velocity from 2D hybrid simulations and 2D MHD simulations of counter-helicity spheromak merging.

- Hybrid simulations of counter-helicity spheromak merging have been compared with MHD simulations.
- For large resistivity (Lundquist number S~500), there were significant differences between hybrid and MHD simulations: in the MHD runs, spheromaks merged completely in about $10t_A$, whereas in hybrid simulations there was no complete reconnection.
- For lower resistivity with S~1500, hybrid simulation results were generally similar to the MHD simulations, and spheromaks were completely merged forming an FRC by t~ $6t_A$.
- Hybrid simulations show shorter current layer and significantly wider velocity profiles.

PPPL
PRINCETON PLASMA PHYSICS LABORATORY

3D MHD simulations in support of MRX flux-rope experiments

(a)

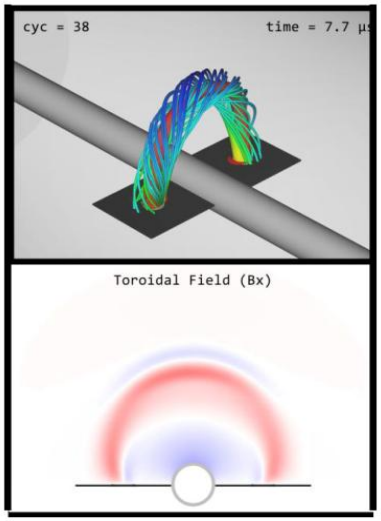

(b)

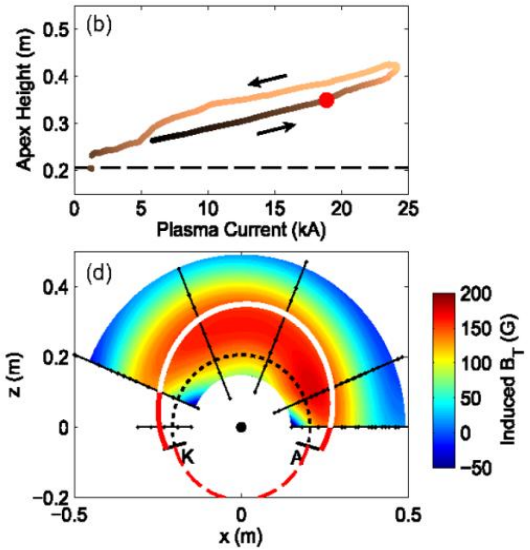

(a) Simulation results showing magnetic field lines and self-generated toroidal field contours of the relaxed configuration;
(b) Experimental results showing dependence of the flux rope expansion on the current strength, and a self-generated toroidal field (C. Myers).

Large toroidal current has been added to external toroidal field at t=0, and configuration was allowed to relax to an equilibrium state.

The goal of the numerical studies is to determine the threshold current below which force balance can be found (without flux-rope eruption) for a given external field configuration, and to guide the design of optimal coil configurations for future experiments on MRX.

PPPL
PRINCETON PLASMA PHYSICS LABORATORY

3D stability simulations (larger V_{beam})

Beam parameters: V_0 =5.6 V_A, v_{th} = 1.5 V_A , n_b = 1% n_0 .

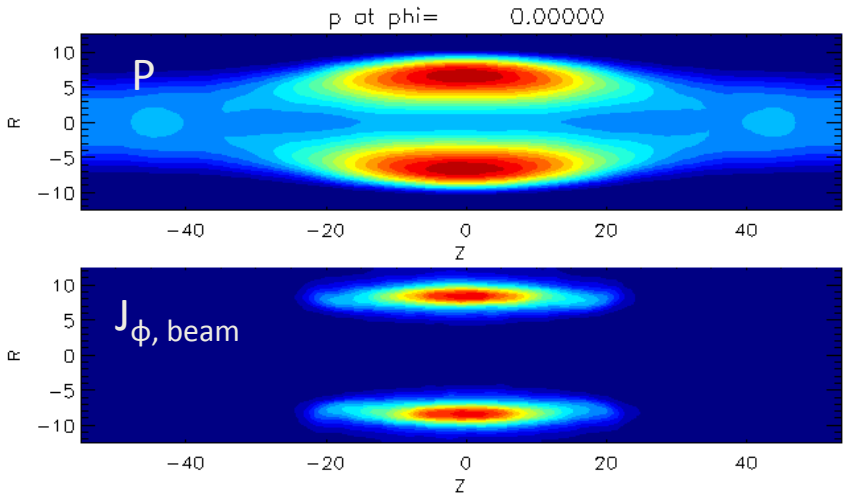

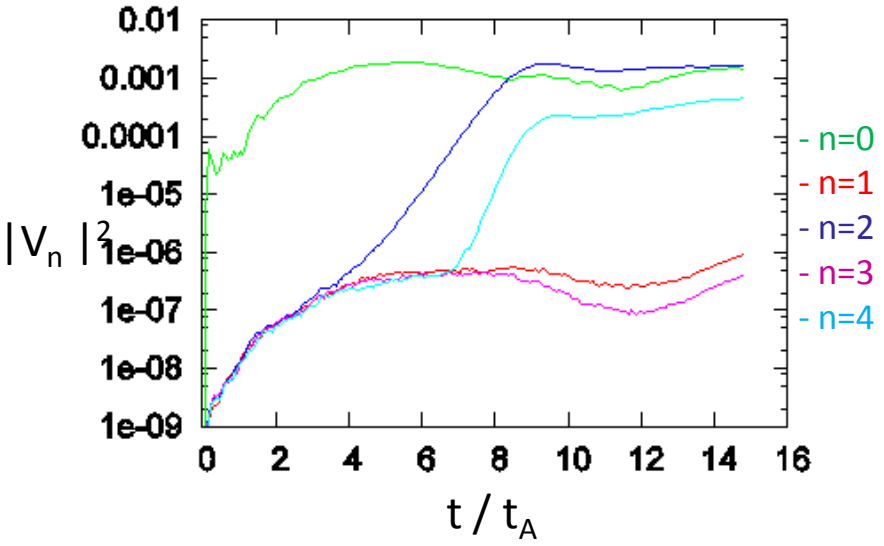

After relaxation, FRC elongates. The beam ions have wider axial profiles for larger v_{th}.

For these beam parameters, the n=1 tilt mode and n=3 modes are completely stabilized, but the n=2 rotational mode is still unstable with $\gamma = \gamma_{mhd}$(n=2) – beam has little effect on n=2 mode.

Generalized energy principle: $\omega_Z, \Omega << \omega_R$

In general, $I = 1/2 \int \delta \boldsymbol{J}_b \cdot \boldsymbol{B}_0 \, x \boldsymbol{\xi}^* \, d^3\boldsymbol{x}$ – self-ajoint provided $\omega << \Omega$ or $\mathrm{Im}(\omega) << \mathrm{Re}(\omega)$.

$$I = \frac{1}{2i\omega^*} \iint (\mathbf{v} \cdot \delta\mathbf{E}^*) \left[-\frac{\partial f_0}{\partial \varepsilon} - \frac{n}{\omega} \frac{\partial f_0}{\partial p_\phi} \right] Int(t) \, d^3\mathbf{v} \, d^3\mathbf{x} - \frac{1}{2 |\omega|^2} \int R \, |\delta E_\phi|^2 \int v_\phi \frac{\partial f_0}{\partial p_\phi} \, d^3\mathbf{v} \, d^3\mathbf{x}$$

where $Int(t) = \int^t (\mathbf{v} \cdot \delta\mathbf{E}) \, dt'$. First term is responsible for resonant interactions, and the resonance condition includes secondary resonances: $n\Omega - \omega = l\omega_Z + m\omega_R$.

For $f_0 \sim \exp(-(\varepsilon - \Omega p_\varphi)/T)$, averaging over radial motion, and assuming modes with odd/even symmetry relative to midplane, it can be shown that [Belova, IAEA 2002]:

$$I_{\mathrm{odd}} = \frac{A_1}{\Omega_n^2 - \omega_Z^{\,2}} + \frac{A_3}{\Omega_n^2 - 9\omega_Z^{\,2}} + \ldots$$

for odd modes
(antisymmetric relative to the midplane,
ie with tilt-like polarization)

$$I_{\mathrm{even}} = \frac{A_2}{\Omega_n^2 - 4\omega_Z^{\,2}} + \frac{A_4}{\Omega_n^2 - 16\omega_Z^{\,2}} + \ldots$$

for even modes
(symmetric, with radial polarization)

where $\Omega_n = n\Omega - \omega$

Generalized energy principle: $\omega_Z << \Omega \sim \omega_R$

Radial resonances are more important for low S* configurations (because $V_b >> v_{th,I}$ implies $\Omega \sim \omega_R \sim \omega_{ci}$), and for modes with even polarization (radial modes).

$$I = \frac{R_0^2 \Omega^2}{2\,|\,\omega\,|^2\,T} \int n_b \frac{|\,\Omega_n\,|^2}{\Omega_n^2 - \omega_R^2} \left| \frac{\partial \delta E_\phi}{\partial R} \right|^2 \delta R^2 d^3\mathbf{x} \sim \frac{1}{\Omega_n^2 - \omega_R^2}$$

where resonant condition: $n\Omega - \omega = \omega_R$.

Dependence of betatron frequencies on S* and Ω_{tor}

S*=20, Ω_0=0.8, n_b/n_0=0.013, J_b/J_0=0.7

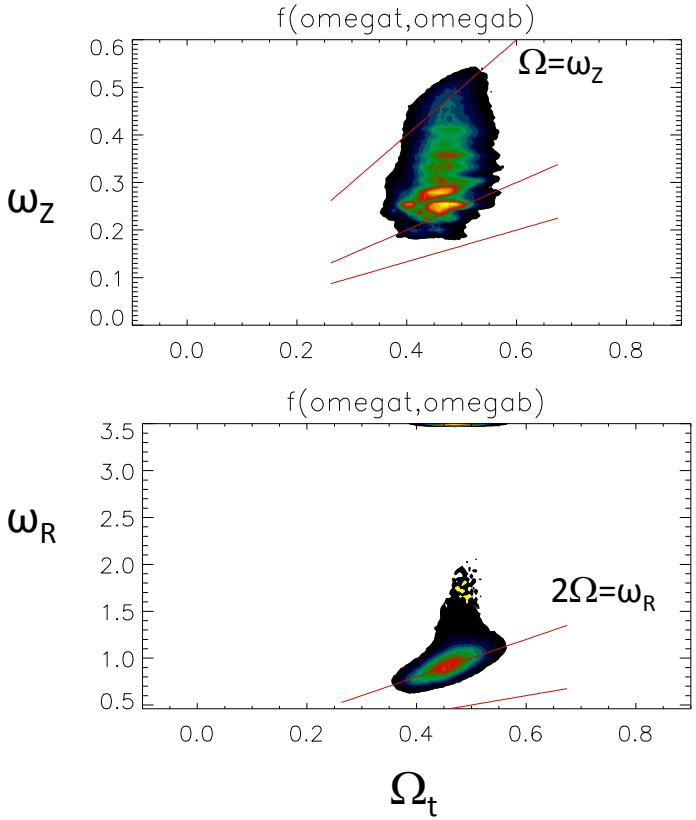

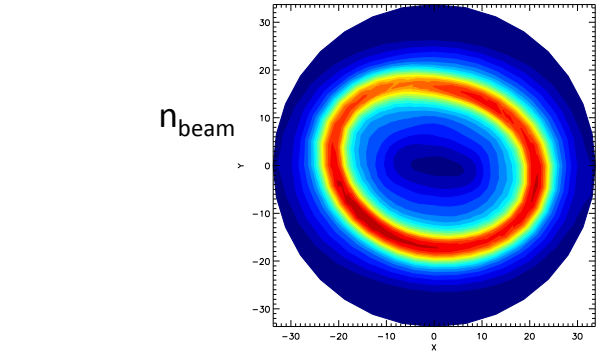

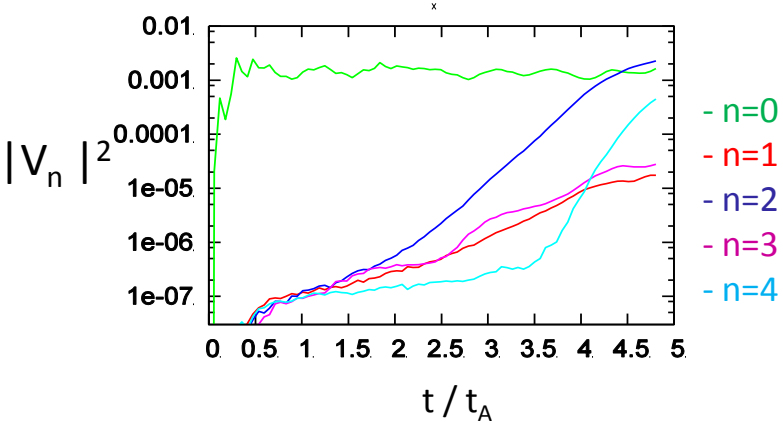

$\omega_Z : \Omega : \omega_R$ = 0.7:1:2

Ratio of radial orbit frequency ω_R to toroidal frequency Ω is $\omega_R / \Omega \sim 2$, and the n=2 mode is the most unstable mode.

Dependence of betatron frequencies on S* and Ω_{tor}

S*=20, Ω_0=0.2, n_b/n_0=0.05, J_b/J_0=0.7

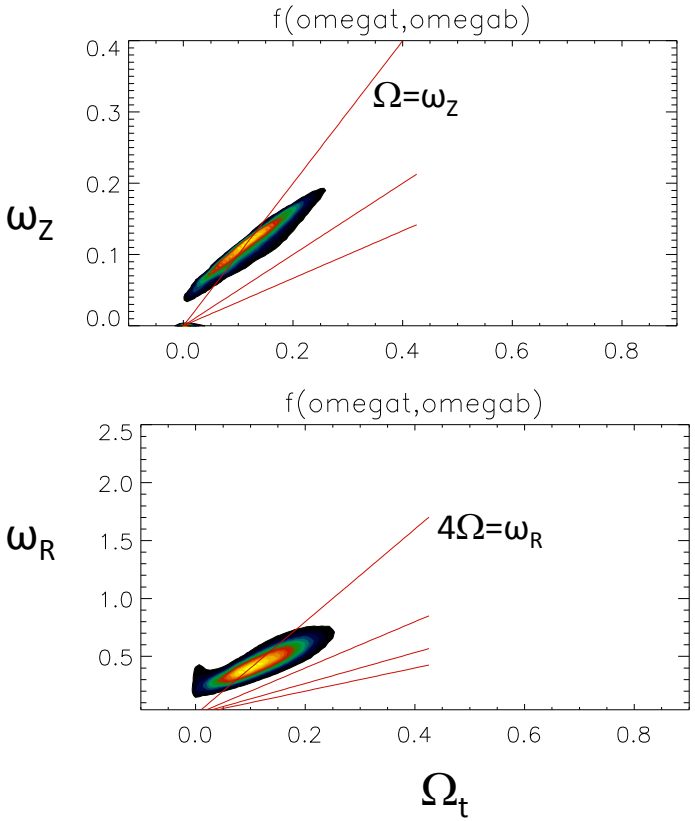

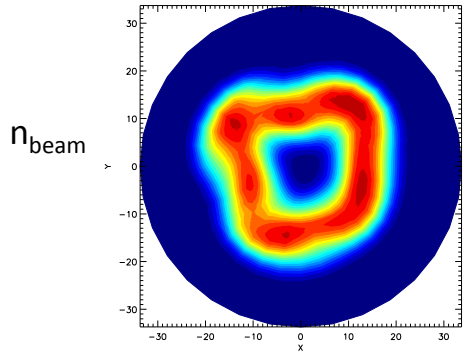

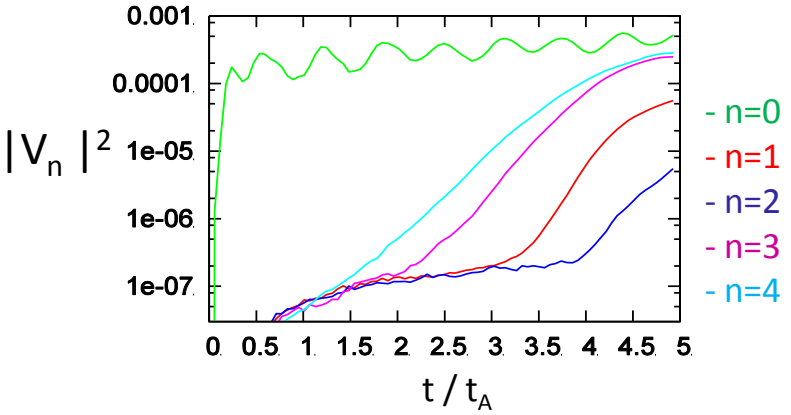

$\omega_Z : \Omega : \omega_R$ = 1:1:4

Ratio of radial orbit frequency ω_R to toroidal frequency Ω is $\omega_R / \Omega \sim 4$, so that resonant condition is satisfied: $\mathbf{n\Omega \approx \omega_R}$ for the n=4 mode.

FRC spin-up due to particle loss and resistive decay (S*=9)

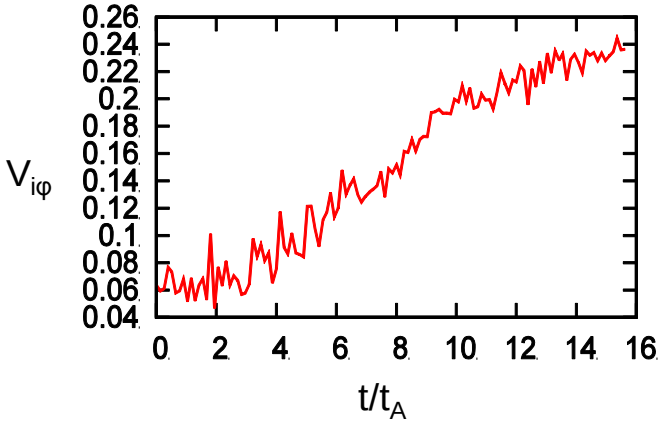

Time evolution of peak ion toroidal velocity inside the separatrix.

Hybrid simulations with n=0 and particle loss boundary conditions show toroidal spin-up with peak ion velocity just outside the separatrix $V_\varphi \sim 0.3V_A$. Most particle from open field lines are lost by $t \sim 10t_A$.

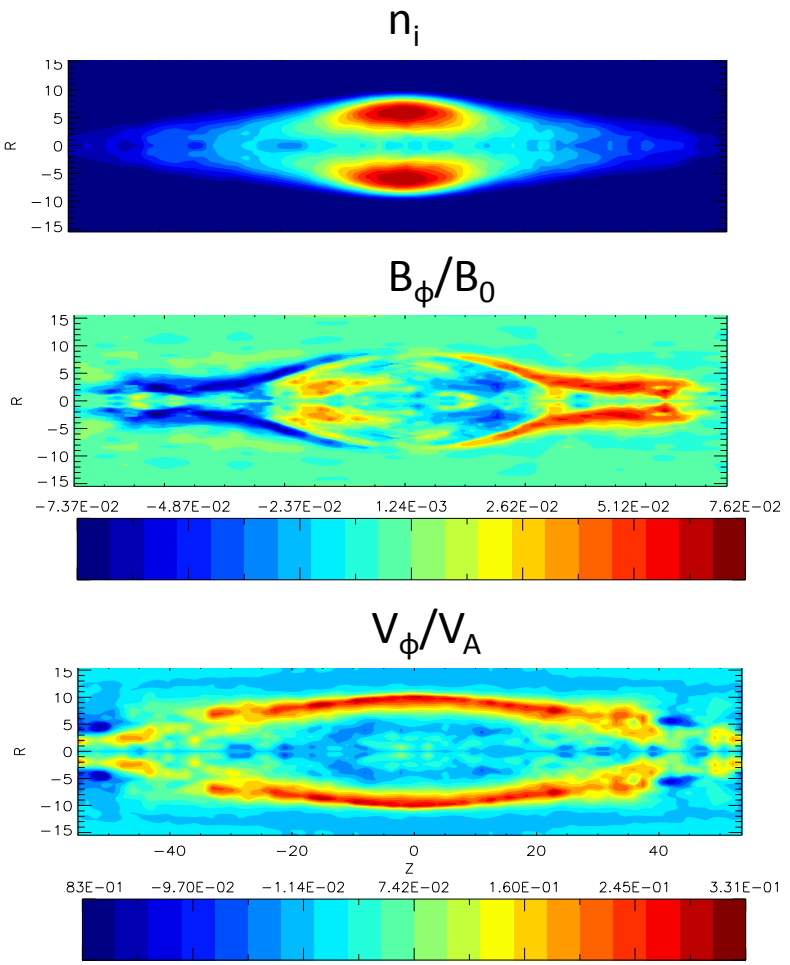

Contour plots of ion density, toroidal field, and toroidal ion velocity at $t=16t_A$.

FRC spin-up: velocity evolution S*=9

t= $10t_A$

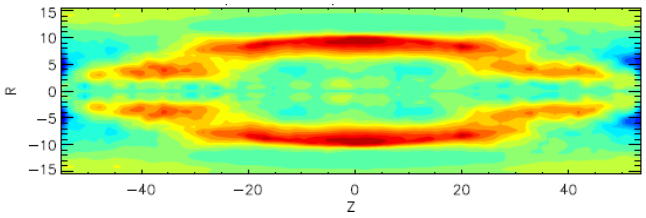

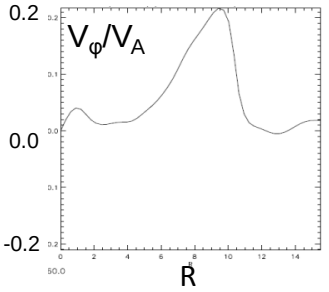

t= $20t_A$

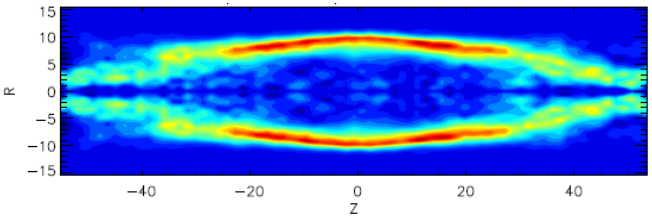

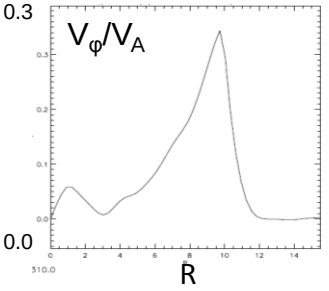

t= $30t_A$

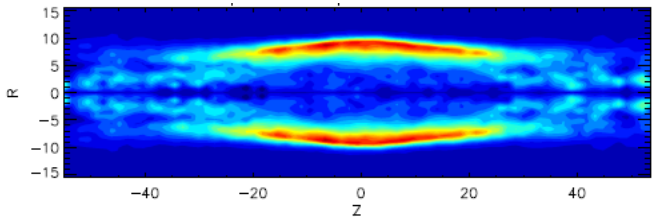

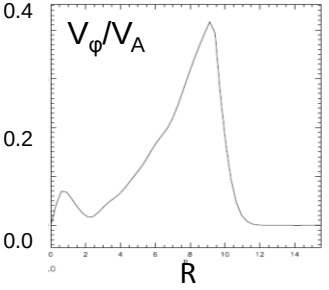

Time evolution of ion toroidal velocity: contour plots and radial profiles of V_ϕ.

Simulations including the particle loss and periodic BCs: n=1 tilt and n=2 rotational mode(S*=9)

- Low plasma resistivity, S~ 4400:
- the n=1 tilt mode is unstable and saturates at t~35t_A, the n=2 rotational mode becomes unstable – no saturation.

- High resistivity, S~ 1500:
all low-n modes are stable for.

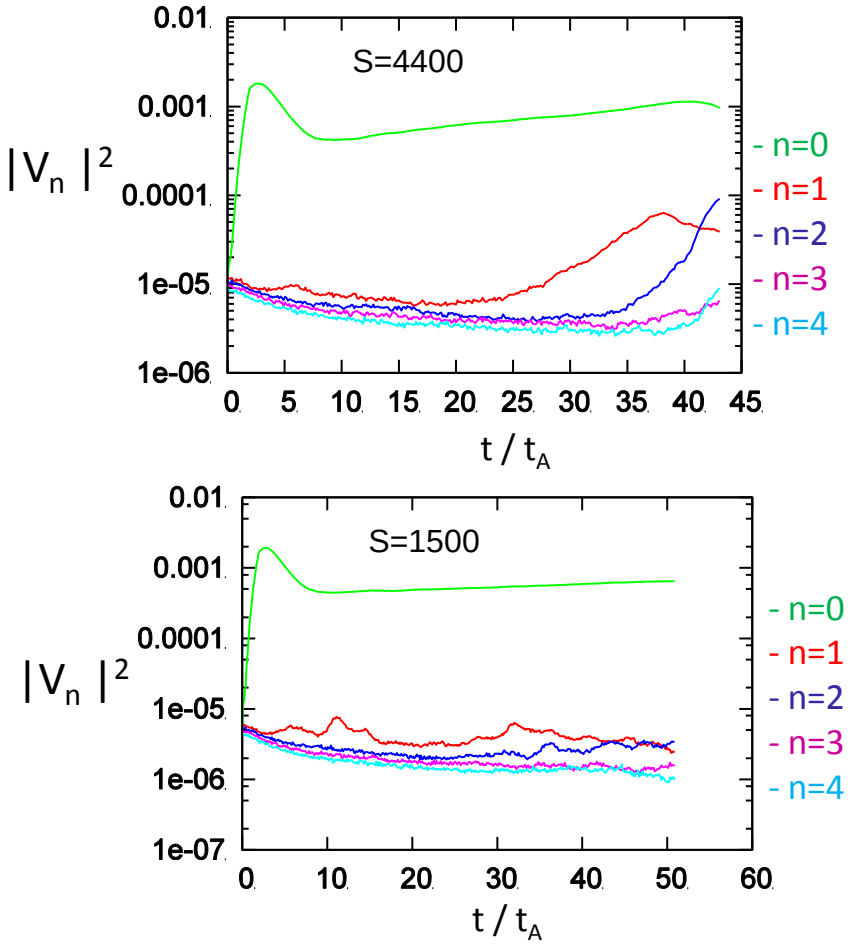

Simulations including the particle loss and end-shorting: unstable n=1 tilt → n=2 rotational mode (S*=9)

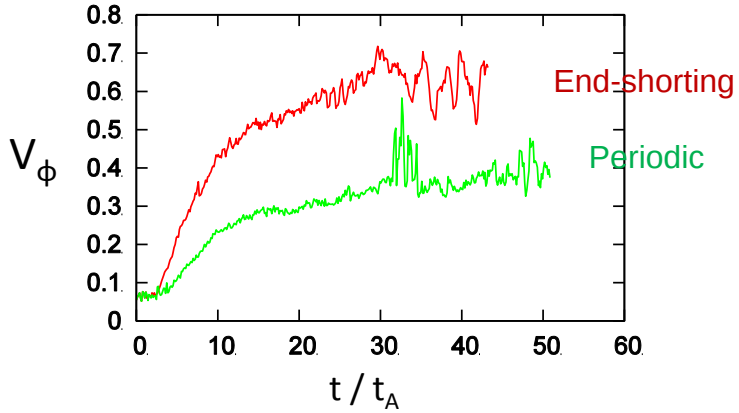

Time evolution of peak ion toroidal velocity inside the separatrix from end-shortening simulations (red) and without end-shorting (green).

- End-shorting results in faster spin-up and instability of n=1 tilt and subsequent growth of the n=2 rotational mode.
- All n=1-4 modes are stable without end shorting for large enough resistivity (periodic BC, no ion rotation at t=0).

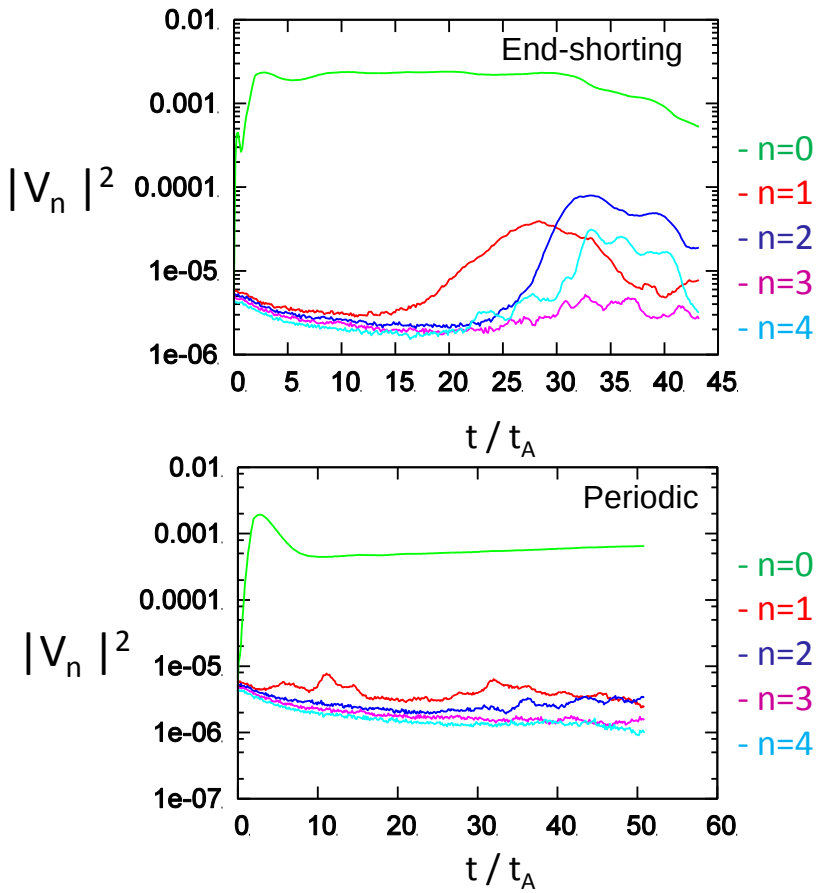

Time evolution n=0-4 mode amplitudes from simulations with particle loss: (a) with end-shortening; (b) without end-shorting. High resistivity, S~ 1500.

Hybrid simulations with fixed $E_R=2*E_0$ at the FRC ends

E_R at FRC end

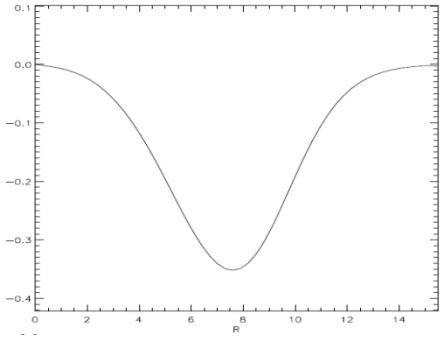

R/λ_i

Profile of electric field applied at the FRC ends. Amplitude was doubled compared to the equilibrium value with no ion rotation.

- When applied E field is doubled compared to the equilibrium value, the n=1 mode becomes unstable at t~10-15t_A. Mode polarization corresponds to radial shift mode (wobble).
- The n=1 tilt and n=2 rotational modes appear to be suppressed.

E_R contours

t~15 t_A

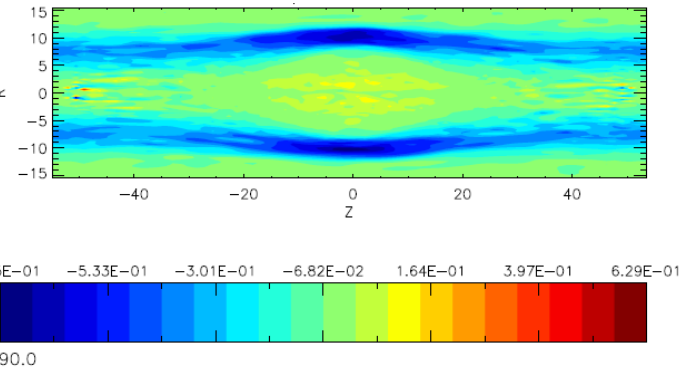

Contour plot of resulting electric field at t=15t_A. Electric field unit in HYM end value ~4.5kV/m, midplane value ~8.5 kV/m.

V_ϕ

t~15 t_A

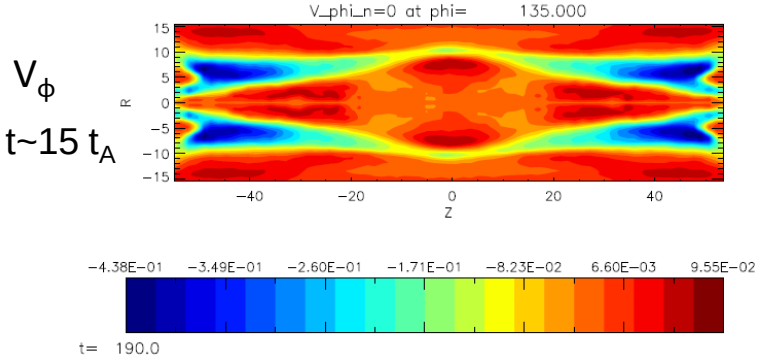

Contour plot of ion toroidal velocity at t=15t_A. There is negative rotation outside separatrix.

Hybrid simulations with fixed $E_R=2*E_0$ at the FRC ends

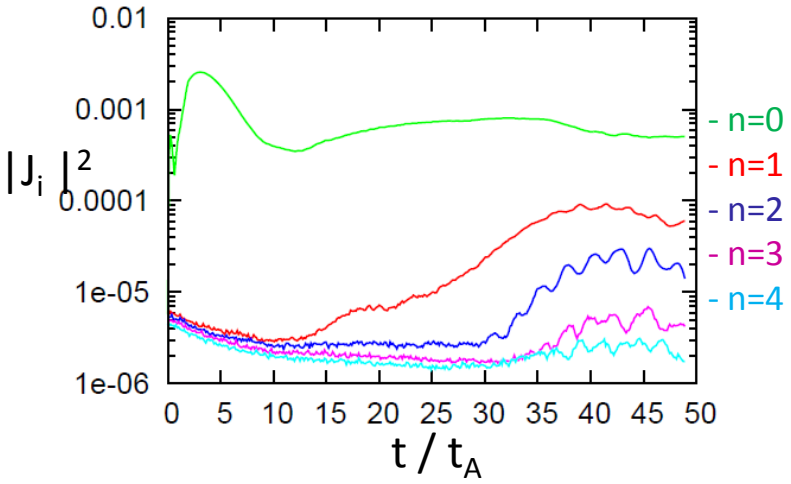

Time evolution n=0-4 mode energies from simulations with end-applied bias field for S*=9.

Perturbed density $t=30t_A$

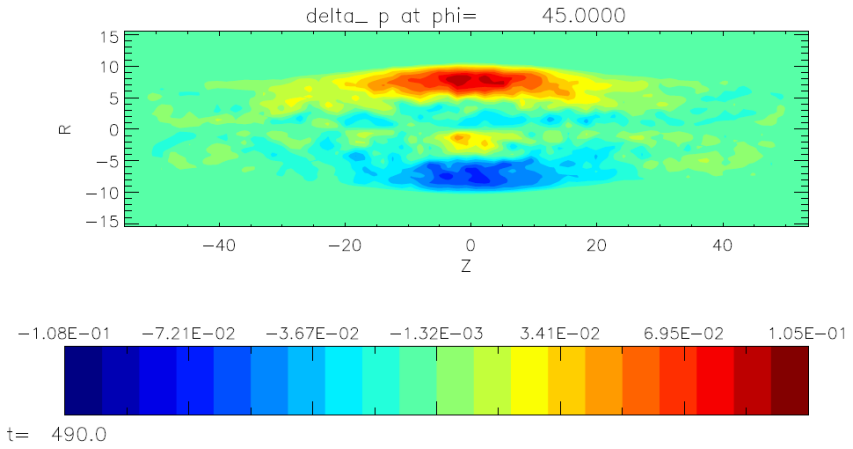

Polarization of unstable n=1 mode corresponds to radial shift mode, as can be seen from δn and δV plots. Perturbed axial velocity is small compared to δV_ϕ and δV_R. Mode rotates in the e-diamagnetic direction with $\omega \sim 0.06\omega_{ci}$.

$t=30t_A$

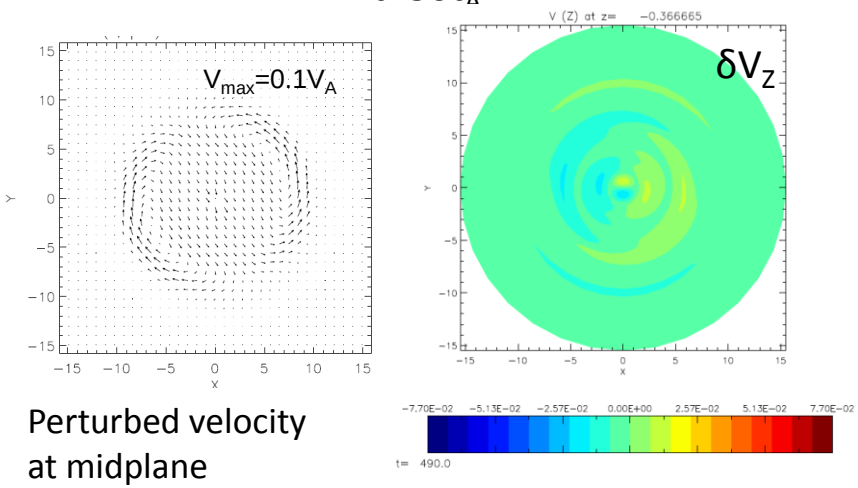

Perturbed velocity at midplane

Non-symmetric BCs: left side – end-shorting, right side – fixed value $E=E_0$.

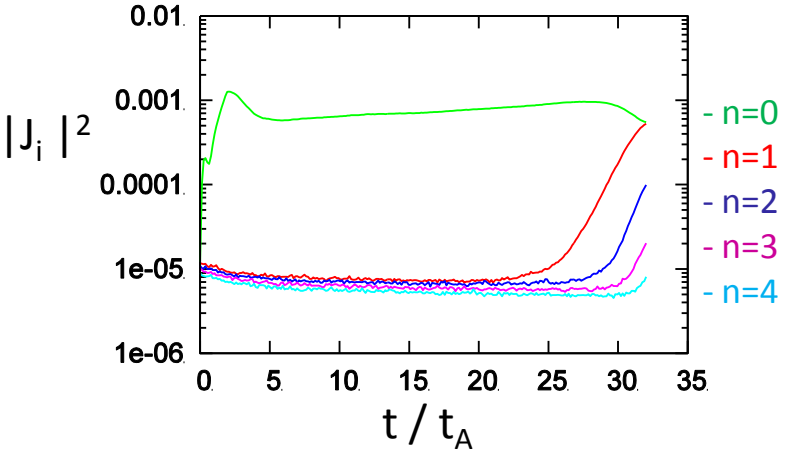

Time evolution n=0-4 mode energies from simulations with non-symmetric boundary conditions. The n=1 mode has radial polarization, ie wobble-like mode.

Toroidal velocity at $t=25t_A$.

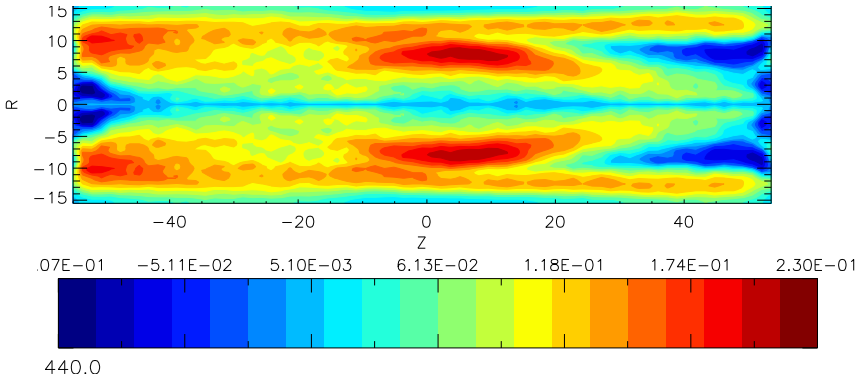

Plasma density at $t=20t_A$ and $t=30t_A$.

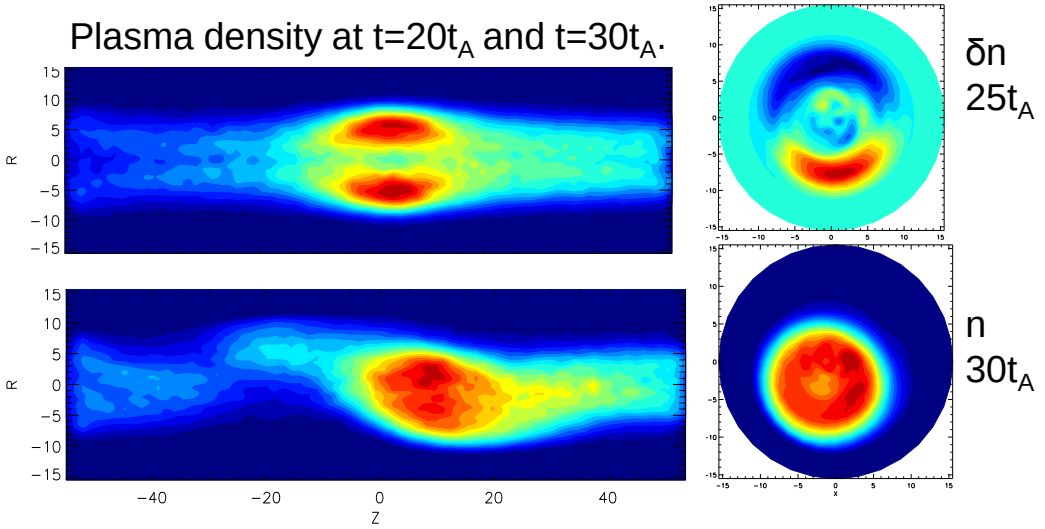

Conclusions (FRC)

- Beam-driven instabilities can be predicted based on energy principle.
- Simulations including the particle loss and periodic BCs show all low-n modes stable for large resistivity.
- End-shorting results in faster spin-up and instability of n=1 tilt and subsequent growth of the n=2 rotational mode.
- When applied E_R field is doubled compared to the equilibrium value, the n=1 mode becomes unstable at t~10-15t_A. Mode polarization corresponds to radial shift mode (wobble).
- Hybrid simulations with non-symmetric BCs with/without end-shorting show strongly unstable n=1 radial shift (wobble) mode.